Research Article | Vol. 26, No. 20 | 1 Oct 2018 | OPTICS EXPRESS 25805
Optics EXPRESS

Video-rate terahertz digital holographic imaging system

M. HUMPHREYS,* J. P. GRANT, I. ESCORCIA-CARRANZA, C. ACCARINO, M. KENNEY, Y. D. SHAH, K. G. REW, AND D. R. S. CUMMING

University of Glasgow, School of Engineering, Microsystems Technology Group, G12 8LT, Glasgow, UK
**m.humphreys.1@research.gla.ac.uk*

Abstract: Terahertz (THz) imaging has been demonstrated in numerous applications from medical to non-destructive evaluation (NDE), but current systems require expensive components, provide slow frame-rates and low resolutions. THz holography offers a potentially low-cost, high-performance alternative. Here we demonstrate the first full video-rate THz digital holography system at 2.52 THz (118.8 μm) using low-cost optical components. 2D digital reconstructions of samples are performed at frame-rates of 50 Hz - an order of magnitude higher than previous systems, whilst imaging of samples concealed in common packaging types demonstrates suitability for NDE applications. A lateral resolution of 250 μm was determined using a 1951 USAF target.

OCIS codes: (090.1995) Digital holography; (090.5694) Real-time holography; (110.6795) Terahertz imaging.

References and links

1. A. Redo-Sanchez, N. Laman, B. Schulkin, and T. Tongue, "Review of terahertz technology readiness assessment and applications," J. Infrared, Millim. Te **34**(9), 500–518 (2013).
2. J. F. Federici, B. Schulkin, F. Huang, D. Gary, R. Barat, F. Oliveira, and D. Zimdars, "THz imaging and sensing for security applications—explosives, weapons and drugs," Semicond. Sci. Technol. **20**(7), S266–S280 (2005).
3. L. Rong, T. Latychevskaia, X. Zhou, H. Huang, D. Wang, and Y. Wang, "Dynamic dehydration observation based on terahertz in-line digital holography," Digital Holography & 3-D Imaging Meeting. (2015).
4. C. J. Strachan, P. F. Taday, D. A. Newnham, K. C. Gordon, J. A. Zeitler, M. Pepper, and T. Rades, "Using terahertz pulsed spectroscopy to quantify pharmaceutical polymorphism and crystallinity," J. Pharm. Sci. **94**(4), 837–846 (2005).
5. C. Baker, T. Lo, W. R. Tribe, B. E. Cole, M. R. Hogbin, and M. C. Kemp, "Detection of concealed explosives at a distance using terahertz technology," Proceedings of the IEEE (IEEE, 2007), **95**(8), 1559–1565**.**
6. L. Liu, W. Fan, X. Chen, and J. Xie, "Identification of high explosive RDX using terahertz imaging and spectral fingerprints," J. Phys. Conf. Ser. **680**, 012030 (2016).
7. I. E. Carranza, J. Grant, J. Gough and D. R. S. Cumming, "Metamaterial-based terahertz imaging," in IEEE Transactions on Terahertz Science and Technology (IEEE, 2015), vol. **5**, no. (6), pp. 892–901.
8. I. E. Carranza, J. Grant, J. Gough and D.R.S. Cumming, "Terahertz metamaterial absorbers implemented in CMOS technology for imaging applications: scaling to large format focal plane arrays,". IEEE Journal of Selected Topics in Quantum Electronics (IEEE, 2017), **23**(4), pp.1–8.
9. F. Simoens, L. Dussopt, J. Meilhan, J. Nicolas, N. Monnier, A. Siligaris, and O. Redon, "Towards industrial applications of terahertz real-time imaging," Proc. SPIE 10531 Terahertz, RF, Millimeter, and Submillimeter-Wave Technology and Applications XI (2018).
10. E. Hack and P. Zolliker, "Terahertz holography for imaging amplitude and phase objects," Opt. Express **22**(13), 16079–16086 (2014).
11. Q. Deng, W. Li, X. Wang, Z. Li, H. Huang, C. Shen, and R. Zou, "High-resolution terahertz inline digital holography based on quantum cascade laser," Opt. Eng. **56**(11), 113102 (2017).
12. M. Locatelli, M. Ravaro, S. Bartalini, L. Consolino, M. S. Vitiello, R. Cicchi, F. Pavone, and P. De Natale, "Real-time terahertz digital holography with a quantum cascade laser," Sci. Rep. **5**(1), 13566 (2015).
13. M. S. Heimbeck, M. K. Kim, D. A. Gregory, and H. O. Everitt, "Terahertz digital holography using angular spectrum and dual wavelength reconstruction methods," Opt. Express **19**(10), 9192–9200 (2011).
14. R. Degl'Innocenti, Y. D. Shah, R. Wallis, A. Klimont, Y. Ren, D. S. Jessop, H. E. Beere, and D. A. Ritchie, "A hybrid plasmonic waveguide terahertz quantum cascade laser," Appl. Phys. Lett. **106**(8), 082101 (2015).
15. TerahertzStore, *https://www.terahertzstore.com/products/terahertz-cameras/terahertz-camera-for-thz-imaging-cea-leti-tzcam.htm*, (2018).

#335552 https://doi.org/10.1364/OE.26.025805
Journal © 2018 Received 19 Jun 2018; revised 3 Sep 2018; accepted 8 Sep 2018; published 19 Sep 2018

Optics EXPRESS

16. V. R Singh and A. Asundi, Digital Holography for MEMS and Microsystem Metrology, chap. 2 (Wiley 2011).
17. Z. D. Taylor, R. S. Singh, D. B. Bennett, P. Tewari, C. P. Kealey, N. Bajwa, and W. S. Grundfest, "THz Medical Imaging: in vivo Hydration Sensing," IEEE Transactions on THz Science and Technology (IEEE, 2011), **1**(1) 12216096.
18. E. Cuche, P. Marquet, and C. Depeursinge, "Simultaneous amplitude-contrast and quantitative phase-contrast microscopy by numerical reconstruction of Fresnel off-axis holograms," Appl. Opt. **38**(34), 6994–7001 (1999).
19. G. Chen, C. Lin, M. Kuo, M. K. Kuo, and C. C. Chang, "Numerical reconstruction and twin-image suppression using an off-axis Fresnel digital hologram," Appl. Phys. B **90**(3-4), 527–532 (2008).
20. C. Mann, L. Yu, C. M. Lo, and M. Kim, "High-resolution quantitative phase-contrast microscopy by digital holography," Opt. Express **13**(22), 8693–8698 (2005).
21. L. Valzania, P. Zolliker, and E. Hack, "Topography of hidden objects using THz digital holography with multi-beam interferences," Opt. Express **25**(10), 11038–11047 (2017).
22. M. K. Kim, L. Yu, and C. J. Mann, "Interference techniques in digital holography," J. Opt. A, Pure Appl. Opt. **8**(7), S518–S523 (2006).
23. P. Girshovitz and N. T. Shaked, "Real-time quantitative phase reconstruction in off-axis digital holography using multiplexing," Opt. Lett. **39**(8), 2262–2265 (2014).
24. J. W. Goodman, "Introduction to Fourier optics, II ed.", McGraw-Hill series in electrical and computer engineering (McGraw-Hill), pp. xviii, 441 p (1996).
25. T. C. Poon and J. P. Liu, "Introduction to modern digital holography: With MATLAB," (Cambridge University 2014).
26. G. D. Boreman and S. Yang, "Modulation transfer function measurement using three- and four-bar targets," Appl. Opt. **34**(34), 8050–8052 (1995).
27. http://dx.doi.org/10.5525/gla.researchdata.627.

1. Introduction

Terahertz (THz) radiation describes electromagnetic radiation with a frequency of between 0.1 and 10 THz. There is widespread research interest in THz radiation due to its properties such as being non-ionizing- thus safe to biological tissue and non-harmful in comparison to x-rays. The ability to remotely penetrate visibly opaque materials such as fabric, paper, cardboard and plastic make it suitable for imaging biological samples (with no sample contact as opposed to ultrasound). It has also proven beneficial for non-destructive evaluation [1] and security applications [2]. The high THz absorption by water allows for dehydration dynamic tests [3] while several materials of interest (including drugs and explosives) have characteristic THz spectroscopic fingerprints [4–6]. Despite significant research effort into developing THz imaging systems, there are still a lack of systems capable of imaging objects in real time for industrial applications. This is largely due to a lack of essential components such as powerful lasers, opto-mechanical components and highly sensitive detectors with sufficient signal to noise ratios (despite emerging devices [7, 8]) at commercially available costs [9].

A useful approach for imaging with THz radiation is to use digital holography which can limit the requirement of custom opto-mechanical components and have the advantage of providing both amplitude and phase information [10]. THz digital holography has been demonstrated at frequencies between 0.7 and 2.52 THz and lateral resolutions of less than 2λ achieved [11–13]. Earlier work using quantum cascade lasers (QCL)- which typically operate at <4 mW of continuous wave emission [14], have been utilized for detection of concealed objects with LWIR microbolometer arrays. The small output beam diameter limits these systems to imaging very small objects, typically only a few mm^2. A higher power laser, implying an increased power density, would allow imaging of larger objects and detection of concealed objects hidden beneath thicker or more absorbing materials. To date, no work has been done demonstrating video rate image capture in real-time.

In this paper, the first THz digital holography system capable of acquiring and reconstructing images at a full camera frame rate of 50 Hz with THz radiation at a frequency of 2.52 THz (118.8 μm wavelength) is proposed. The system is based around a CO_2 pumped CH_3OH FIR laser and can be used to identify concealed objects in several types of packaging at a stand-off distance of 15 mm, whilst also allowing larger objects to be imaged. Only commercially available components are used in this system where the total LWIR microbolometer focal plane array (FPA) detector and optics cost (ignoring the source cost) is

Optics EXPRESS

an order of magnitude less than current state of the art THz microbolometer FPAs [15]. Reconstruction speed is increased through the use of an efficient multiplexing algorithm taking advantage of graphics processing units (GPUs), to allow reconstruction an order of magnitude faster than previous holography systems [13].

A reflection holographic system based around the off-axis holography configuration is used [16]. The reflection mode has been previously demonstrated to be beneficial for imaging highly absorbent materials with THz radiation - particularly biological samples [17]. It also allows for easy separation of the amplitude and phase information [18] and separation of the zero-order mode compared to in-line holography systems whilst also providing further advantages such as noise reduction [19] and ability to measure sub-wavelength changes in optical thickness [20]. THz imaging has been proven for concealed metallic objects [21] and our system demonstrates this with two common packaging materials.

2. Experiment

The holography system was assembled in an off-axis reflection holography configuration as shown in Fig. 1. An FIR CH_3OH laser pumped by a CO_2 laser (Edinburgh Instruments FIR-295) was used as the source emitting ~100 mW at a wavelength of 118.8 µm (2.52 THz). Standard plano gold mirrors (Thorlabs) and a high resistivity float zone (HRFZ) Si beam-splitter (Tydex) were used for the optics. Figure 1(a) shows the off-axis reflection setup whilst Fig. 1(b) shows the Computer Aided Design (CAD) drawing of the aluminium sample which was placed approximately 15 mm away from the detector. This detector distance allowed enough space for the reference beam to combine with the object beam at the detector without interacting with the sample object.

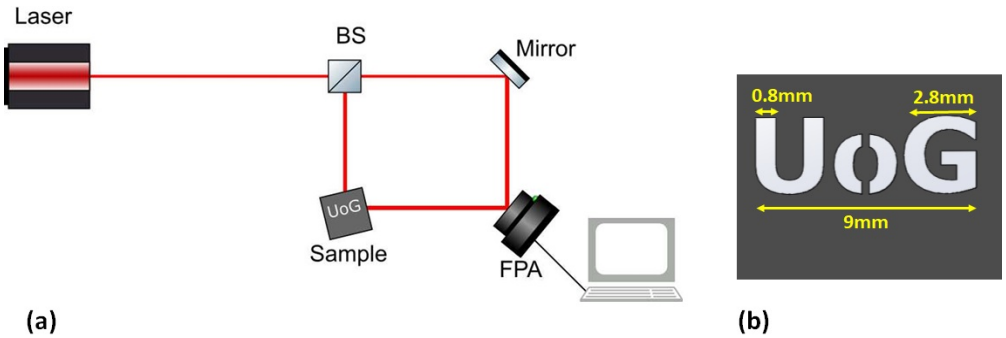

Fig. 1. (a) Experimental set-up of the off-axis reflection holography system and (b) CAD drawing of the aluminium sample object.

The detector used was an uncooled LWIR microbolometer array (Xenics Gobi-640) designed for the 8-14 µm wavelength range with 640x480 pixels at 17 µm pixel pitch. The detector was connected to a commercially available PC (AMD Ryzen 7 1700x CPU with 8-3.4 GHz cores and two NVidia Titan XP GPUs with SLI bridge) via a Teledyne Dalsa frame grabber which transferred data at a frame rate of up to 50 Hz. This was interfaced with Matlab via the image acquisition toolbox and used Matlab's GPU array capabilities through the parallel computing toolbox to increase the reconstruction frame rate and take advantage of the two GPUs. We used the angular spectrum reconstruction method [14] along with a hologram multiplexing algorithm to obtain real-time reconstruction of the holograms. Using a motorized *x,y,z* axis translation stage, the same sample was scanned and reconstructed at a 50 Hz frame rate.

The angular spectrum reconstruction method requires two Fast Fourier Transforms (FFTs) as opposed to the standard Fresnel reconstruction method and hence needs more computing power, however it offers more flexibility in that there is no minimum distance requirement between the object and hologram plane [22]. The angular spectrum describes the 2D Fourier

Optics EXPRESS

Transform of a wavefield in the *x*-*y* plane propagating in the *z* plane. This can be denoted as wavefield *W(x,y,z)* with corresponding angular spectrum *A(α/λ,β/λ,z)* where α and β are the *x* and *y* directional cosines corresponding to the spatial frequencies of *W(x,y,z)*. Choosing *z* as the distance between the sample object and hologram plane allows for the angular spectrum at the detector to be found when the FFT of the angular spectrum is multiplied by the propagation kernel in Eq. (1):

$$A\left(\frac{\alpha}{\lambda},\frac{\beta}{\lambda},z\right)=A\left(\frac{\alpha}{\lambda},\frac{\beta}{\lambda},0\right)\exp\left(j\frac{2\pi}{\lambda},\sqrt{1-\alpha^2-\beta^2}z\right) \tag{1}$$

The FFT of Eq. (1) gives the wavefield of the original object *H(x,y,z)*. To obtain a successful digital reconstruction of the original object, digital filtering to remove the second and zero order terms must be applied along with digital simulation of the reference wave to recover the real image. The reference wave, *R*, at the off-axis angle, θ, used to form the real image can be simulated using Eq. (2):

$$R(\theta)=\exp\left(j\frac{2\pi}{\lambda}y\cdot\sin(\theta)\right) \tag{2}$$

After multiplying *H(x,y,0)* by *R(θ)*, the zero order mode and the mirror image wavefield can be filtered out by applying a circular filter of zeros to the FFT in Fourier space. Back-propagating the real object wavefield using Eq. (1) and applying the inverse FFT gives the filtered reconstruction of the original object *O(x,y,z)*. The full steps for the reconstruction process are described in algorithmic form by Eq. (3)

$$O(x,y,z)=inverseFFT\left[backpropagation\left(FilteredFFT\left(H(x,y,0)\right)\right)\right] \tag{3}$$

This can also be described in integral form as shown in Eq. 4.1 - 4.4 where matrix *C* represents the circular filter of zeros, f_x and f_y are the spatial frequencies in the x/y directions, whilst BP represents the back propagation kernel.

$$Y\left(f_x,f_y\right)=\left[C\right]\Big|_{z=0}\cdot\iint e^{-j2\pi(f_x x+f_y y)}\cdot H(x,y,0)\cdot dx\cdot dy \tag{4.1}$$

$$f_{zo}=\sqrt{1-(\lambda\cdot f_x)^2-(\lambda\cdot f_y)^2} \tag{4.2}$$

$$BP=e^{j\frac{2\pi}{\lambda}\mathbb{R}\{f_{z0}\}\cdot z} \tag{4.3}$$

$$O(x,y,z)=\frac{1}{2\pi}\iint e^{j2\pi(f_x+f_y)}\cdot BP\cdot Y(f_x,f_y)\cdot df_x\cdot df_y \tag{4.4}$$

3. Real time digital holography algorithm

In order to perform a fast hologram reconstruction, the GPUs were used with the Matlab GPU functionality to improve processing speed. Additionally, a hologram multiplexing algorithm, as designed by Girshovitz [23], was employed to maximize efficiency. The first hologram read from the camera (frame *n*) and the next (frame *n* + 1) were summed together (after frame *n* + 1 was rotated 90°) and the Fast Fourier Transform (FFT) of the cross correlation taken, before cropping to increase the processing speed of the inverse FFT. Here the 1st order modes of frames *n* and *n* + 1 are cropped for faster elimination of unwanted terms and faster inverse FFT performance. This allowed for full camera frame rates (50 Hz) to be reconstructed. A summary of the algorithm is shown in Fig. 2. The time taken to reconstruct 100 frames from an '.avi' file was 2.104s (47.5 fps). Reconstructing 300 frames took 5.7s (52.6 fps) and similar frame rates were achieved for any number of frames larger than this. When testing the speed from a live data stream from the frame-grabber reconstructions were performed at a steady rate at 50 fps - the native speed of the camera stream and bottleneck speed for the

Optics EXPRESS

system. This compares favorably (around twice the frame-rate) to state-of-the-art THz FPAs [15].

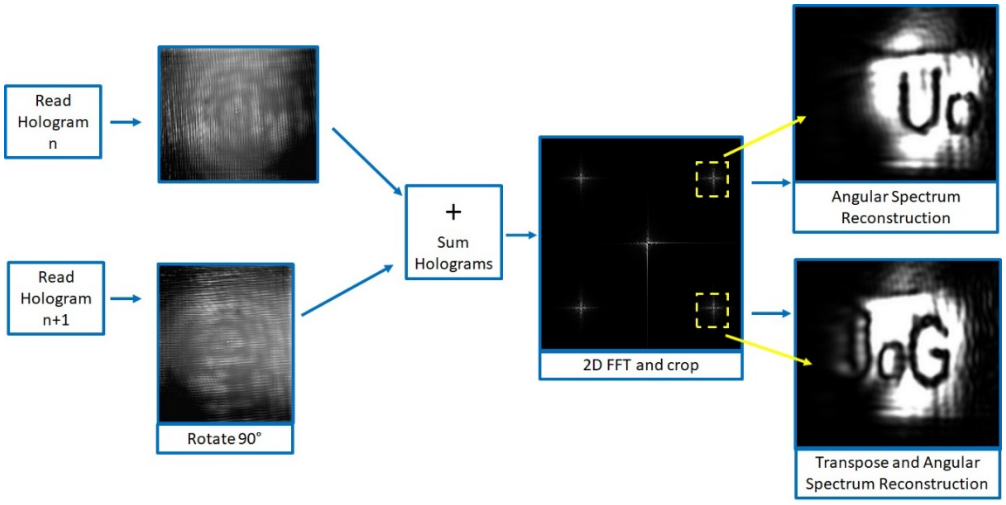

Fig. 2. Hologram multiplexing algorithm for real time reconstruction.

4. Simulations

4.1 Propagation

Simulations with Matlab were used to aid with the system design, understanding of the interference patterns and test the reconstruction algorithms. In order to initially simulate the propagation and interferogram at the detector, the Fresnel-Kirchhoff integral convolution method was applied to an image of the sample object [24]. To mimic the THz laser source, a Gaussian beam with a wavelength of 118.8 μm and 20 mm diameter was applied. Sampling with the same pixel pitch and number of pixels as the Gobi 640 camera used experimentally was also applied to the simulation. The reconstruction of the amplitude was obtained using the angular spectrum algorithm described in section 2.

4.2 Optimizing resolution

In a holographic imaging system, the maximum achievable resolution is determined by the sensitivity, pitch and number of pixels of the camera along with the off-axis angle, θ. The distance between the detector and the object significantly affects the resolution, with a closer distance allowing a better resolution. Therefore, a larger off-axis angle provides the benefit of easier alignment by allowing more space between the reference beam and object beam to ensure they only cross at the hologram plane, allowing for the smallest possible object-detector distance to be used. Consequently, the choice of θ also determines the Numerical Aperture (NA) of the system. The largest off-axis angle that can be used is dependent on the detector with an optical transfer function (*OTF*) described by Eq. (4) [25]:

$$OTF \propto \left| F\left[rect\frac{x}{w} \right] \right|^2 \propto \sin c^2(p \cdot f_x) \tag{4}$$

Where there are 640 pixels in the *x*-axis and 480 in the *y*-axis for the camera used, f_x is spatial frequency at x, and p is pixel pitch = 17 μm. The cut-off frequency f_{cutoff}, for the camera was found with a fringe spacing of 6.92 cycles/mm which can be used along with the wavelength (in mm) to find the maximum off-axis angle θ_{max} (in degrees) using Eq. (5):

Optics EXPRESS

$$\theta_{\max} = \sin^{-1}\left(f_{cutoff} \cdot \lambda\right) \tag{5}$$

For a source wavelength of λ = 118.8 µm (0.1188mm), the maximum off-axis angle for the set-up was θ_{max} = 55.3°. This relatively large maximum angle allowed for greater separation of the real, mirror and zero order terms. Using this angle resulted in using a working distance of 15 mm between object and detector with a 7 mm imaging area giving an NA of 0.23. The system could be designed to have a larger working distance, but at the expense of resolution.

5. Results

A sample object was made from 1 mm thick aluminum containing laser cut features with a 0.8 mm width. Each letter had a total width of 2.8 mm as shown in Fig. 1(b). The interferogram and reconstruction were simulated using the CAD file of the sample object as well as the previously described propagation and reconstruction methods. The resulting interferogram, spectra and amplitude reconstruction can be seen in Fig. 3.

The experimentally obtained interferogram, frequency spectra and amplitude reconstruction captured from the Gobi-640 camera can be seen in Fig. 4. Differences between the simulated and experimental interferogram are thought to be caused by the beam profile not being perfectly Gaussian, some reflections at the camera plane, and thermal noise that couldn't be easily removed along with crosstalk between pixels in the FPA. Note the interferogram is stitched together from two interferograms in order to portray the full 9 mm wide sample with the aforementioned 7 mm imaging area. In order to demonstrate that the system could capture a moving video image the object was scanned across the field of view in the x-y plane at a rate of 2 mm/s using a computer controlled translation stage. A video-rate image was reconstructed in real-time at 50 fps (see Visualization 1). The intensity changes in the reconstruction of Fig. 4 (right) are largely due to the instability of the gas laser consequently affecting the beam profile.

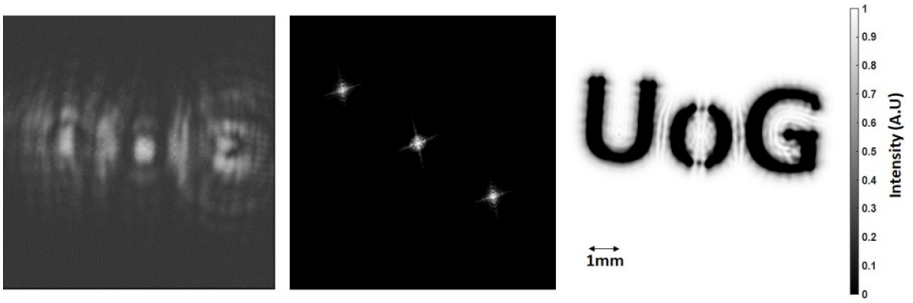

Fig. 3. Simulated interferogram (left), frequency spectrum (mid) and amplitude reconstruction of sample (right).

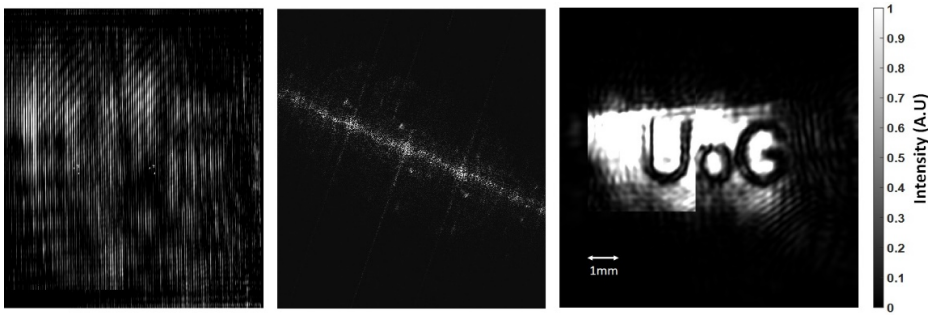

Fig. 4. Experimental interferogram (left), frequency spectrum (mid) and amplitude reconstruction of sample (right).

Optics EXPRESS

To evaluate the system for suitability as a package inspection tool, the sample object was concealed within two of the most common packaging materials; (1) a paper envelope and (2) a standard polythene delivery package. Figure 5 shows the resulting amplitude reconstructions which retain all of the features of the object due to THz being highly transmissive within these media. There is small amount of image quality degradation compared to the uncovered sample in Fig. 4 due to noise caused by slight reflections from the packaging, but the features remain clear.

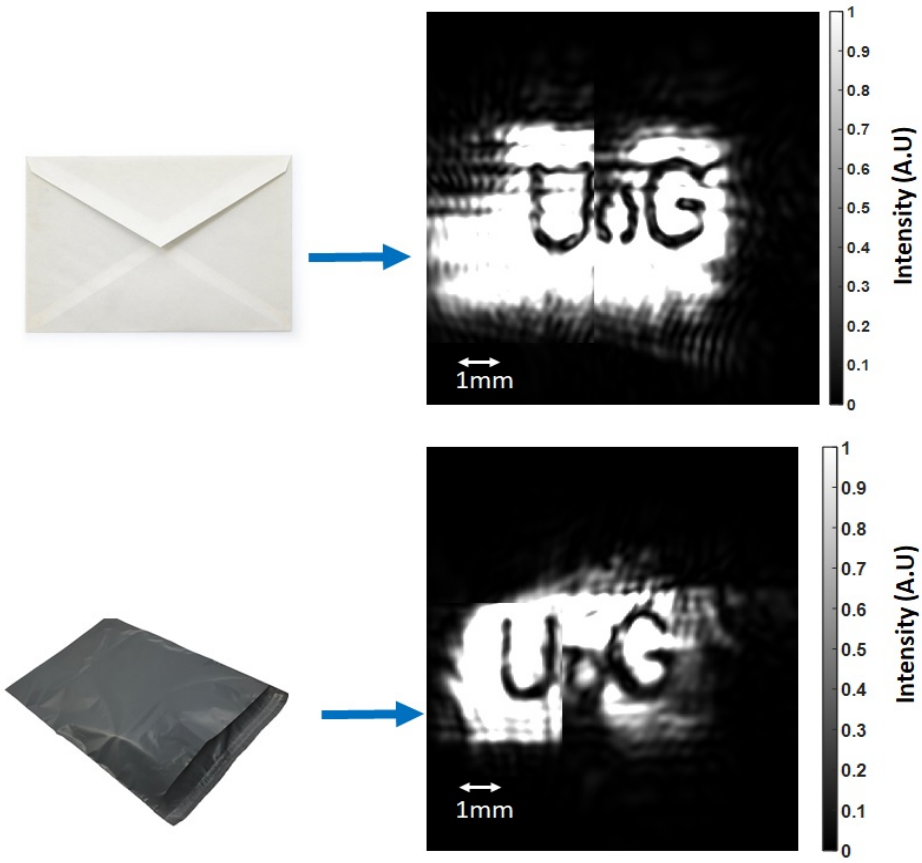

Fig. 5. Reconstruction of the UoG object concealed in a paper envelope (top) and polythene package (bottom).

In order to determine the smallest feature size the system could resolve, a 38 mm diameter clear path, nickel 1951 USAF target (Edmund Optics) was imaged. Figure 6(a) shows an optical image of the object whilst Fig. 6(b) shows the reconstructed amplitude hologram of the object stitched from several holograms of the different sections whilst Fig. 6(c) shows a zoom of the smallest group of lines that can be clearly resolved which equates to 3.5 lines/mm or 280 µm. The vertical dotted yellow line represents the cross-section region used in Fig. 6(d) which is the intensity plot across the smallest group of lines to prove this resolution. This matches well with the resolution of other holography systems at this wavelength [10, 13]. This could be improved through use of a detector with a smaller pixel pitch and larger number of pixels (larger detector area).

The modular transfer function (MTF) was obtained for the sample by using Boreman's method for finding MTF of three bar targets [26] and is shown in Fig. 7. The 10% modulation level occurs at 4 lines/mm or 250 µm.

Optics EXPRESS

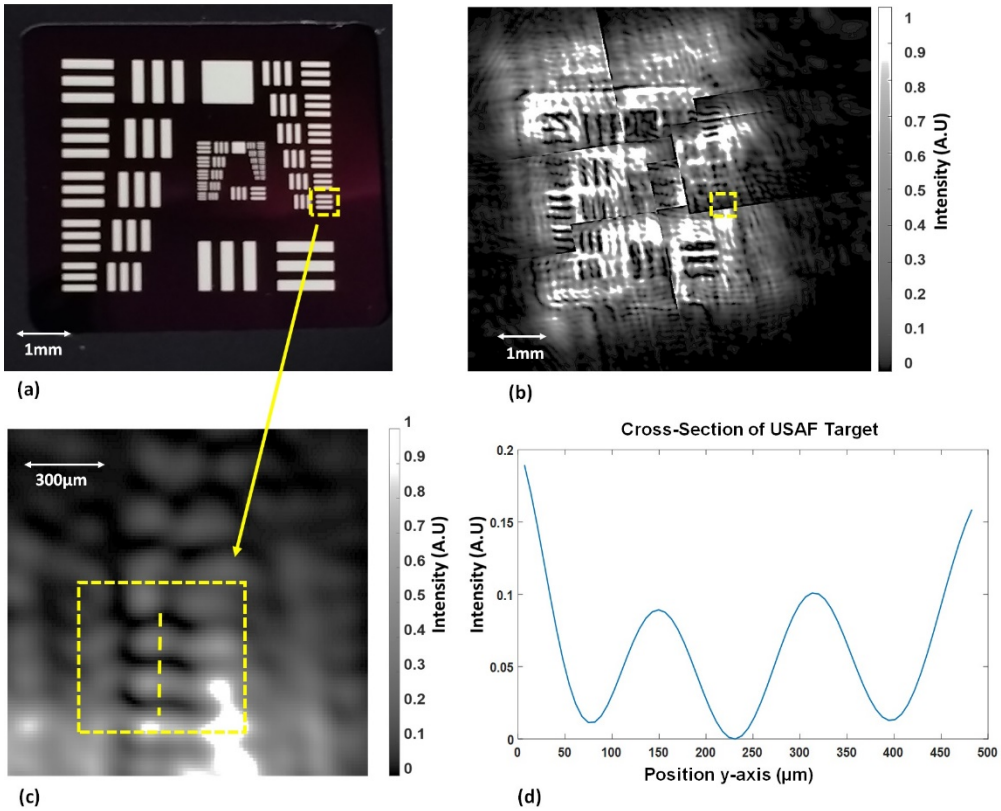

Fig. 6. (a) Optical image of 1951 USAF target sample, (b) amplitude reconstruction hologram and (c) zoom of the highlighted region. Feature sizes of 2λ were resolved (d) Intensity plot of cross section of highlighted region.

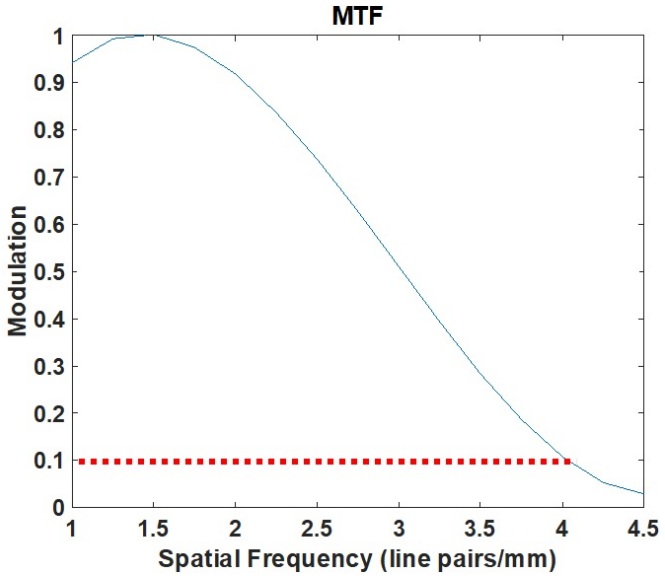

Fig. 7. Plot of MTF for USAF target.

Optics EXPRESS

6. Conclusions

We have demonstrated a real time THz digital holography system capable of imaging moving objects at a frame rate of 50 Hz and resolving features smaller than 280 μm. The application of imaging metallic objects concealed in common packaging types was also demonstrated highlighting suitability for remote sensing and non-destructive evaluation applications in industrial quality control and security imaging. The system demonstrated provides a versatile and low-cost alternative to current state-of-the-art real-time THz cameras for fast 2D scanning of concealed objects.

The system's lateral resolution is limited by the pixel pitch and number of pixels (larger detector area) of the camera and the stability of the laser source (consistent phase) as well as the distance between the object and detector. Development of high power THz QCLs would allow for more stable holograms and greater quality of images. Use of a highly tuneable laser would allow for dual wavelength reconstruction in order to eliminate 2π ambiguities in phase unwrapping to allow depth measurements of objects thicker than half wavelength without prior object knowledge. Low-cost FPAs with better sensitivity at THz frequencies, smaller pixel sizes and lower noise would significantly improve the resolution, imaging area, field of view and overall performance.

Funding

Engineering and Physical Sciences Research Council (EP/L016753/1, EP/J018678/1).

Acknowledgments

We thank Grant Quinn from School of Engineering IT Support at University of Glasgow for his help with the computing specification and support.

We thank Martin Heimbeck and Henry Everitt of University of Alabama for sharing their advice, information and sample code. We also thank Lorenzo Valzania from Empa Swiss Federal Laboratories for Materials Science and Technology, for his excellent advice and support.

Author acknowledges the support from the EPSRC Centre for Doctoral Training in Intelligent Sensing and Measurement (Grant No. EP/L016753/1).

The data set associated with this research is available at [27].